Internal hydraulic jumps and overturning generated by tidal flow over a tall steep ridge

Sonya Legg[1] and Jody Klymak[2]

[1] Program in Atmosphere and Ocean Sciences

Princeton University, 201 Forrestal Road, Princeton, NJ 08544, USA,

Sonya.Legg@noaa.gov

[2] School of Earth and Ocean Sciences, University of Victoria,

P.O. Box 3055 STN CSC, Victoria, B.C., Canada, V8W 3P6,

jklymak@uvic.ca

Submitted to Journal of Physical Oceanography

February 6, 2008

Abstract

Recent observations from the Hawaiian ridge indicate episodes of overturning and strong dissipation coupled with the tidal cycle near the top of the ridge. Simulations with realistic topography and stratification suggest that this overturning has its origins in transient internal hydraulic jumps which occur below the shelf-break at maximum ebb-tide, and then propagate up the slope as internal bores when the flow reverses. A series of numerical simulations explores the parameter space of topographic slope, barotropic velocity, stratification and forcing frequency, to identify the parameter regime in which these internal jumps are possible. Theoretical analysis predicts that the tidally-driven jumps may occur when the vertical tidal excursion is large, which is shown to imply steep topographic slopes, such that $dh/dxN/\omega > 1$. The vertical length-scale of the jumps is predicted to depend on the flow speed such that the jump Froude number is of order unity. The numerical results agree with the theoretical predictions, with finite amplitude internal hydraulic jumps and overturning forming during strong offslope tidal flow over steep slopes. These results suggest that internal hydraulic jumps may be an important mechanism for local tidally-generated mixing at tall steep topography.

1 Introduction

The flow of barotropic tides over ocean topography may lead to the generation of internal tides and mixing, a topic of much recent interest following observations that about 30% of tidal dissipation occurs in the open ocean (Egbert and Ray, 2000). It is believed that some of this energy loss results in mixing that could drive the thermohaline circulation (Wunsch and Ferrari, 2004). Several recent field programs have examined the role of tide-topography interactions in leading to this tidally-generated mixing at oceanic topography which may take the form of multiple irregular ridges, such as the fracture zones around the Mid-Atlantic ridge (Polzin et al., 1997) or isolated steep ridges, such as the Hawaiian ridge (Rudnick et al. (2003), Klymak et al. (2006)), and on continental slopes (Nash et al., 2007). These observations have shown that tidal energy is both converted into internal waves, which radiate away from the topography, and used for local mixing at the topography. In order to develop new energetically consistent parameterizations of tidal mixing for global climate models, the physical processes governing the transfer of energy from barotropic tide to baroclinic motion to mixing need to be fully understood. This article describes one physical process by which tidal flow over isolated topography leads to local mixing, namely internal hydraulic jumps, and explores the parameter regime over which this behavior is possible.

As a prelude to this study, it is helpful to understand the degree to which the parameter space of tidal flow over isolated topography has been examined to date. For a single ridge, the controlling dimensional parameters are ω, the tidal frequency; N, the buoyancy frequency; f the Coriolis parameter; h_0, the topographic height; H the water depth; L, a horizontal lengthscale associated with the topography; and U_0, the amplitude of the barotropic current (Garrett and Kunze, 2007; Legg and Huijts, 2006). From these a suitable choice of governing nondimensional parameters

consists of: the frequency ratios, ω/f and ω/N; the tidal excursion distance normalized by the topographic lengthscale, $U_0/(\omega L)$; the relative height of the topography, h_0/H; and

$$\gamma = h_0/(Ls) \text{ where } s = \left(\frac{\omega^2 - f^2}{N^2 - \omega^2}\right)^{1/2} \tag{1}$$

so that γ is the ratio of the topographic slope to the slope of the internal tide characteristic. We will refer to γ as the topographic steepness, where supercritical slopes have $\gamma > 1$ and subcritical slopes have $\gamma < 1$. Another important parameter, although not independent of those listed, is the topographic Froude number

$$Fr = \frac{U_0}{Nh_0} \tag{2}$$

which is a measure of the obstruction of the flow by the topography; in steady flows, strongly nonlinear lee-waves are generated for $Fr < 1$. Previous studies have examined the influence of increasing γ and h_0/H on the character of the internal tides and the energy conversion (Balmforth et al. (2002), Llewellyn Smith and Young (2003), Khatiwala (2003), St Laurent et al. (2003)), and shown that energy conversion is increased by a factor of 2 as γ increases from infinitesimally small to ∞, and increased still further as $h_0/H \to 1$. $U_0/(\omega L) > 1$ has been shown theoretically and numerically (Bell (1975), Legg and Huijts (2006)) to lead to generation of internal tides at higher harmonics of the forcing frequency.

While theoretical studies have proved useful in predicting the energy conversion rate, they are unable to examine regimes with finite amplitude barotropic forcing, and the partitioning of energy between local mixing and radiated internal tides. In Legg (2004) and Legg and Huijts (2006) the parameter space of large $U_0/(\omega L)$ combined with small $U_0/(Nh_0)$ has been shown numerically to lead to the possibility of nonlinear hydraulic effects which may be one source of local mixing. Another source of local mixing is the rapid dissipation of internal tides of small vertical scale, which

are generated when $\gamma > 1$, with a greater proportion of energy in smaller wavelengths if h_0/H is small.

In this article we examine further the possibility for mixing associated with internal hydraulic jumps in a somewhat different regime, where $U_0/(\omega L)$ is small, but where strongly nonlinear transient lee-waves with overturning similar to internal hydraulic jumps may form if the Froude number associated with the vertical tidal excursion distance is small.

The parameter space we are concerned with in this paper is motivated by observations made close to topography on Kaena Ridge during the Hawaiian Ocean Mixing Experiment (Levine and Boyd, 2006; Aucan et al., 2006; Klymak et al., 2007). The top left panels of figures 1 and 2 show two tidal cycles of observations made from FLIP near the top of the shelf-break. While the total water depth in this location is about 1000m, FLIP observations only extended down to 800m. Interesting features of the observations include a sudden increase in density at around the time the current, dominated by the M2 tide, changes sign, accompanied by almost vertical isopycnals with overturning and high values of dissipation. The enhanced dissipation and steepened isopycnals extend well above the topography and are clearly linked to the tidal cycle. Since the observations are made only in a single location, it is difficult to identify the physical mechanism by which the tide leads to this overturning and dissipation from these observations alone. We are therefore motivated to carry out a numerical and theoretical study, whose purpose is to identify these mechanisms, linking the processes taking place at this location with those at other locations around this topography, and identifying the necessary criteria for this phenomenon to exist, so that the understanding gained from the Hawaiian ridge can be generalized to other areas of the global ocean.

The Hawaiian ridge falls into the region of parameter space characterized by $\gamma > 1$, $U_0/(\omega L) << 1$, and $U_0/(Nh_0) << 1$, i.e. region 5 in the parameter space diagram of Garrett and Kunze

(2007). The specific values of these parameters when the barotropic flow amplitude is around $5cm/s$ are $\gamma \approx 4$, $U_0/(\omega L) \approx 0.01$ (corresponding to a horizontal tidal excursion of around 350m) and $U_0/(Nh_0) \approx 0.006$. h_0/H is large, i.e. $h_0/H \approx 0.8$.

2 Model set up

In our model study we employ the MITgcm (Marshall et al., 1997), integrating the nonhydrostatic Boussinesq equations in a 2D configuration similar to that described in Legg and Huijts (2006) and Khatiwala (2003). A nonhydrostatic model is preferable since previous studies (e.g. Legg and Adcroft (2003)) have shown that highly nonlinear internal bores, associated with rapid increases in density, which may be responsible for the density perturbations seen in the observations, are poorly represented by hydrostatic models. Simulations in only 2-dimensions are a reasonable first step for this topography since at the Hawaiian ridge the flow is constrained to go over the topography through a channel between islands, and cannot go around the topography instead. The relative inexpense of 2-dimensional simulations also allows us to perform a comprehensive parameter space investigation, so that we can identify the controlling physical processes.

The MITgcm is a height-coordinate model which represents topography through a finite volume formulation, and includes a free-surface. In order to investigate the physical mechanisms responsible for the features described in the observations, several different calculations, with different topography, stratification, forcing amplitude and forcing frequency are carried out. The key parameters of all the simulations described in this paper are given in the Table, including several non-dimensional quantities. The initial stratification is horizontally uniform; in the *Realistic* experiment that stratification is taken from observations at the Hawaiian ridge, while in all the other

simulations stratification is constant. In most of the simulations $N^2 = 5.69 \times 10^{-6} s^{-2}$ (shown in figure 3a), while four calculations vary N^2 to be 2×, 4×, 8× and 1/4 of this value. A linear equation of state is employed. The model domain is 500km across and 4300m deep. The central portion of the model contains a single topographic feature; in the *Realistic* simulation a smoothed version of the actual topography at the Kaena ridge is used, while other simulations use an idealization of this topography, consisting of a well-defined steep slope to the left, a flat shelf, and a more gentle slope to the right. The idealized topography has the analytic form:

$$h(x) = -H + h_0 exp\left(-\frac{(x + w/2)^2}{2L^2}\right) \; ; \; x < -w/2 \tag{3}$$

$$h(x) = -H + h_0 \; ; \; -w/2 < x < w/2 \tag{4}$$

$$h(x) = -H + h_0 - \alpha_2 (x - w/2) \; ; \; w/2 < x < w/2 + h_0/\alpha_2 \tag{5}$$

$$h(x) = -H \; ; \; x > w/2 + h_0/\alpha_2 \tag{6}$$

where w, the width of the flat peak of the topography, is 16km. L, the width of the slope, is chosen to give a desired maximum steepness, $dh/dx_{max} = (h_0/L)exp(-0.5)$ which varies from 0.2 for the *Steep* topography down to 0.06 for the *Gentle* topography. α_2 is the slope of the right hand slope, set to 0.04 in all the idealized calculations, much less than the average slope of the *Realistic* simulation. Given that the wave characteristic slope is $s = 0.05$, this right hand slope is therefore just less than critical. The different topographies are shown in figure 3.

The barotropic tidal forcing $U = U_0 sin(\omega t)$ is applied through a body-forcing term at the M2 tidal frequency ($\omega = 1.41 \times 10^{-4} s^{-1}$), with a deep water velocity amplitude U_0 of 2, 5, or 10 cm/s. Observational values vary from 2 to 5 cm/s over the course of the spring-neap cycle. Three other calculations have a forcing frequency of 2×, 3× and 0.5× the M2 frequency (in the latter case Coriolis is reduced so that we remain in the regime where propagating waves can exist at the

forcing frequency).

The resolution is variable in both horizontal and vertical directions, as shown in figure 4, with a minimum gridsize over the top of the slope of $\Delta x = 115m$ and $\Delta z = 8.8m$. The maximum Δx near the boundaries of the domain is $3km$, while the maximum Δz, at depth, is $49.3m$, with a total number of grid points in the horizontal and vertical directions of $nx \times nz = 1000 \times 300$. Laplacian friction is employed in the momentum equations, with horizontal and vertical components of viscosity set to $\nu_h = 10^{-1} m^2/s$ and $\nu_v = 10^{-2} m^2/s$, these being the values necessary to prevent grid-scale noise in the velocity fields. These values are certainly much larger than realistic ocean values, being chosen for numerical rather than physical reasons, and the simulations will therefore be at a lower Reynolds number than the ocean, implying more viscous damping of the flow. Comparison with observations will allow us to evaluate this aspect of the model. The Superbee flux-limiting advection scheme for tracers introduces numerical diffusivity where needed to eliminate grid-scale noise, so the explicit tracer diffusivities are set to zero. Again, the numerical diffusion is introduced for numerical reasons rather than as an attempt to model the physical mixing, and hence we do not expect the model mixing efficiency to match that which would be observed. For this reason we do not use the model to calculate quantities such as diapycnal mixing in this study. Previous studies (Legg and Adcroft, 2003) have shown that the model mixing efficiency is considerably reduced compared to values measured for similar scenarios in the laboratory. These limitations of the model should not however affect its ability to model nonlinear waves, and we therefore focus on this aspect of the simulations.

No-flux boundary conditions are applied to tracers at the free-surface and at the bottom topography, while no-slip boundary conditions are applied to momentum at the topography. The side boundaries employ an Orlanski radiative boundary condition for the baroclinic flow, and specified

boundary values for the barotropic flow (Khatiwala, 2003). All simulations are started from rest, and continued for 5.6 M2 tidal periods. The Coriolis parameter has a constant value of $f = 8.0 \times 10^{-5} s^{-1}$ (except for the $\omega/2$ case where $f = 2.0 \times 10^{-5} s^{-1}$). This is larger than the actual value of Coriolis in the Kaena ridge region ($5.4 \times 10^{-5} s^{-1}$) because parametric subharmonic instability (PSI, which may occur for $2f < \omega$, Gerkema et al. (2006)) is not the focus of this particular study, and so f is set high enough to prevent it from occurring in the M2 forcing frequency calculations (the two calculations at higher forcing frequency are susceptible to PSI however). Other aspects of the real ocean which we are ignoring for this study are horizontal variations in stratification, and multiple tidal frequencies. Obviously a full understanding of the tide-topography interaction would require examination of these complications; however, our purpose here is to understand a single process in isolation.

3 Results

3.1 Realistic simulation

We first focus on the comparison between the observations and the results from the simulation with Realistic topography and stratification, shown in the Top center panels of the figures 1 and 2. Like the observations, the model results show sudden increases in density at the time the flow changes direction from off- to on-slope, coinciding with steep isopycnals and enhanced dissipation. This suggests that the model is to first order capturing the phenomena responsible for this overturning and dissipation. A principal difference between the model and observations is the reduced magnitude of the isopycnal displacements and dissipation in the model, probably a result of excessive numerical

damping in the model. Despite these quantitative differences, the model results can be regarded as qualitatively capturing the features, and therefore provide guidance on their origin.

The source of these features can be identified by examining the behavior simulated by the model further down the slope. Figure 5 shows a sequence of snapshots of the cross-slope flow and density, beginning near maximum off-slope flow, and ending near maximum onslope flow. At maximum off-slope flow, there is a strong downslope flow, with isopycnals plunging sharply downward adjacent to the slope, followed by a sudden rebound. This feature is strongly reminiscent of an internal hydraulic jump, or a strongly nonlinear quasi-stationary leewave (Farmer and Smith, 1980). When the flow begins to relax, the jumplike feature moves towards the slope, and in successive snapshots, propagates up the slope as an internal bore associated with strong convergent flow and overturning isopycnals. This internal bore seems the likely cause of the overturning and dissipation seen in the observations from FLIP above the shelf-break.

To further examine the behavior associated with the passage of the internal bore on the slope, we show time-depth profiles of cross-slope velocity, dissipation, stratification and shear at a location down on the slope where the water depth is -1150m (figure 6). This is located within the region of plunging isopycnals during the downslope flow. At this deeper location, there is a noticeable bottom enhancement in the off-slope flow. High dissipation is found near the boundary, which near the time of the flow reversal extends about 250m above the topography. This vertical extent is considerably greater than the height of the maximum shear in the downslope flow (about 50m above the bottom). The high dissipation extending above the bottom coincides with greatly weakened stratification, including overturned isopycnals, centered on about -1000m depth.

To summarize, the results for this particular topography show enhanced downwelling on the left flank of the topography, associated with a hydraulic jump-like feature. When the flow relaxes, the

flow reversal is associated with low stratification (including overturning characterized by negative stratification), and high dissipation. The flow reversal and associated overturning and mixing propagate up the slope as an internal bore, weakening as they go.

3.2 Sensitivity of nonlinear features to physical parameters

These hydraulic jump-like features and the overturning and dissipation associated with them depend on the external parameters of topographic slope, stratification, flow amplitude and forcing frequency. In figures 1 and 2 the velocity, density and dissipation are shown for model simulations with idealized topography, and varying slopes and tidal forcing amplitude. The *SteepU5* simulation has linear stratification and an idealized topography, with values chosen so that the stratification is equal to that at the shelfbreak in *Realistic*, and the maximum topographic steepness is equal to that in *Realistic*. The results are very similar to those in *Realistic*, suggesting that the idealized simulation reproduces the main physical parameters responsible for this behavior. The snapshots of cross-slope velocity and density shown in figure 7 (a) and (b) also confirm the similar behavior in the *Realistic* and *SteepU5* simulations, with overturning internal bores visible in both.

With the idealized topography, we can examine the sensitivity of the behavior to the topographic steepness, by varying the parameter L in equation 3. For the *Medium* slope, similar internal bore features are seen (figures 7c and 1,bottom left); however for the *Gentle* slope, there is no evidence of internal bores or enhanced dissipation associated with the change in flow-direction (figures 7d and 1,bottom center). Slope steepness is therefore evidently a necessary ingredient for the formation of the internal bores.

Tidal flow amplitude also influences the response. For weak flow *SteepU2*, while overturns and

enhanced dissipation are still seen (figures 7e and 1,bottom right), they are of smaller amplitude. For stronger flow *SteepU10*, the vertical extent of the overturning is greatly enhanced (figure 7f).

In the interest of brevity, we do not show snapshots or timeseries for the simulations with different stratification and forcing frequency, since these all look similar to other simulations. Simulations with varied stratification all show internal hydraulic jumps and overturning, but on lengthscales that increase as stratification is decreased. Simulations with increased forcing frequency show less marked overturns, so that with a frequency of 3ω, the structures have many similarities to those seen with the *Gentle slope*.

At a single location on the slope, the passage of the internal bores is seen by a rapid decrease in buoyancy, followed by a more gradual increase. A quantification of this asymmetry is the skewness of the time-derivative of buoyancy, shown for all simulations in figure 8. A negative skewness in $\partial b/\partial t$ corresponds to rapid decreases in buoyancy, with more gradual increases. At $h = -1150m$ there is no consistent tendency for the skewness, while at $h = -1028m$, all except two cases show a negative skewness over the bottom 200m of the profile, near the topography. This is similar to that seen in Legg and Adcroft (2003) when upslope propagating bores are generated by reflection of low mode internal tides from near-critical slopes. This supports the proposal suggested by the snapshot sequence that the internal hydraulic jumps/lee-waves generated during the offshore flow give rise to upslope propagating bores when they encounter the slope following the flow relaxation. The simulations which do not show any negative skewness are those where bores are not seen, i.e. when slope is very gentle (*GentleU5*), or forcing frequency is very large (3ω).

A measure of the vertical extent of the overturning associated with the passage of the internal bores is the region affected by low gradient Richardson number (fig. 9). The highest location where $Ri = 1$ is shown as a function of time for a location of topographic depth $h = -1150m$, for all

simulations. Steeper slopes and higher amplitude forcing are associated with greater vertical extent of the low Richardson number region. For increasing ω the height of low Ri increases with time, and for 3ω is displaced above the bottom, associated with mid-depth shear, possibly due to the development of PSI, not the jump-like regions seen in other simulations. Reducing (increasing) stratification leads to a greater (lesser) vertical extent of overturning, as the displacement scale increases (decreases).

Dissipation, calculated from $\nu_i(\partial u_j/\partial x_i)^2$, shown in figure 10, is concentrated along the internal tide characteristics emanating from the critical points at the top of the two flanks of the topography, and following reflection, from the surface. In most of the calculations an additional region of enhanced dissipation is seen at the top of the left flank, where the slope is close to critical. Exceptions to this occur when the slope is closely aligned with the wave slope (fig 10d) or the forcing amplitude is small (fig10e).

In summary weaker amplitude forcing (*SteepU2*) leads to a smaller region of low Richardson number, as well as a smaller peak in dissipation, with dissipation at the top of the topography not significantly larger than on the internal tide beams. Stronger forcing (*SteepU10*) enhances the features seen in *Steep slope* and extends the overturning over a greater vertical extent. The slope steepness, s, has a strong influence. In the *Gentle slope* case the flow is much more linear with only a small low-Richardson number region, lower dissipation and no negative skewness in the buoyancy time-derivative. Both significant steepness downstream of the topographic peak and large amplitude forcing therefore appear to be necessary to produce significant local overturning. Stratification and forcing frequency also influence the development of internal jumps, with decreasing stratification leading to larger vertical lengthscales, and increasing ω reducing the appearance of the jumps.

4 Interpretation in terms of internal hydraulics

Having shown qualitatively that large steepness and large amplitude flow both enhance the strength of overturning internal bores, we will now quantify these relationships by developing theoretical predictions for (a) the regime in which tidally generated internal hydraulic jumps may occur; (b) the magnitude of the vertical displacements associated with the tidal flow.

In single layer hydraulic control theory, a flow is supercritical if the flow speed is greater than the single-layer long wave phase speed: $U > \sqrt{g'H}$, where U is the flow speed, g' is the buoyancy anomaly of the layer and H is the layer depth. Long gravity waves cannot propagate upstream in a supercritical flow. Hydraulic control occurs when the flow transitions from subcritical to supercritical as it flows over a topographic obstacle, so that downstream of the obstacle peak the flow is fast, and fluid layer is thin compared to their upstream values. Often a second transition from supercritical to subcritical occurs downstream of the obstacle, in the form of a hydraulic jump (Long, 1953, 1954).

Continuously stratified flows over topography are considerably more complicated, because the internal wave horizontal phase velocity may take on an infinite number of values. The maximum phase velocity corresponds to the lowest vertical mode; if the flow speed exceeds this maximum phase velocity all modes will be unable to propagate against the flow. The Hawaiian ridge topography does not fall in this regime for realistic barotropic velocities. Instead it may fall into a regime in which larger wavelengths can propagate while smaller vertical wavelengths are arrested. An alternative viewpoint in which to consider this regime is that of the lee-waves which occur in steady flow over topography. It is instructive to consider the conditions under which lee-waves become highly nonlinear and overturn: when the Froude number $Fr = U/(Nh_0)$ (where h_0 is the amplitude

of the topography) is equal to, or less than unity, a regime of highly nonlinear, breaking lee-waves occurs, in which the overturning bears some resemblance to an internal jump. Durran (1986) has shown that the flow structure in the breaking region also resembles a supercritical flow. Our scenario differs strongly from these atmospheric studies in that our forcing velocity is time-dependent, and our topography extends close to the surface of a finite-depth ocean rather than through a small extent of a very deep atmosphere. Nonetheless, it is useful to consider our jump-like features as perhaps transient analogues of the highly nonlinear overturning lee-waves seen when $Fr < 1$.

An oscillating flow with $U/(\omega L) << 1$ (as it is in these calculations where the width of the ridge, L, is 30km for the realistic topography) will only experience a small fraction of the full topographic height during an oscillation period. This contrasts with steady-state flows which are influenced by the full height of the topography. For the oscillating case, in the absence of stratification the distance a parcel is advected down the slope during the tidal cycle is the vertical excursion distance:

$$Z_\omega = \frac{U_0}{\omega} dh/dx \tag{7}$$

The Froude number based on this vertical distance is

$$Fr_{Z_\omega} = \frac{U_0}{NZ_\omega} = \frac{\omega}{Ndh/dx} \tag{8}$$

By analogue with steady flows, we would therefore expect to see highly nonlinear, jump-like transient lee-waves only if the vertical excursion distance is sufficiently large that

$$Fr_{Z_\omega} = \frac{\omega}{Ndh/dx} < 1 \tag{9}$$

The maximum displacement of an isopycnal is a convenient measure of the nonlinearity of flow response to the topography, and might be expected to scale with the vertical excursion distance:

$$\Delta h \sim Z_\omega \tag{10}$$

If we nondimensionalize Δh by U_0/N (the maximum displacement allowed on energetic grounds) then this scaling relationship would be

$$\Delta h N/U_0 \sim dh/dx \frac{N}{\omega} = Fr_{Z_\omega}^{-1} \tag{11}$$

In figure 11 we show the maximum vertical displacement Δh of isopycnals originating above the shelf, nondimensionalized by U_0/N, plotted against $Fr_{Z_\omega}^{-1}$. Δh has been diagnosed from all the different simulations in which U_0, ω, dh/dx and N are varied. The schematic shown in figure 12 shows an example of the measured Δh. In the region of 11 where $Fr_{Z_\omega}^{-1} < 3$, there is a linear relationship, as predicted in equation 11. For low $Fr_{Z_\omega}^{-1}$ therefore, this scaling holds, and the correlation coefficient between Δh and Z_ω is $R = 0.97$ for these low $Fr_{Z_\omega}^{-1}$ points. However, for that part of figure 11 where $Fr_{Z_\omega}^{-1} > 3$, a different scaling applies: in this regime $\Delta h N/U_0$ is approximately constant, and has a value of about 10. For these high $Fr_{Z_\omega}^{-1}$ points, the correlation coefficient between Δh and U_0/N is $R = 0.94$.

There are therefore two distinct regimes, with $Fr_{Z_\omega}^{-1}$ being the regime-controlling parameter, as suggested by the theoretical scaling analysis. For low $Fr_{Z_\omega}^{-1}$, i.e. shallow slopes, weak stratification, high frequency forcing, the tide reverses before the stratification suppresses vertical motions, and Δh is just set by the vertical tidal excursion. The waves in this regime are linear with little overturning. For high $Fr_{Z_\omega}^{-1}$, i.e. steep slopes, strong stratification, low frequency forcing, the tide lasts long enough for stratification to work against the downslope motions, and Δh scales like U_0/N. The U_0/N scaling gives a maximum value of Δh permitted on energetic grounds; when the Z_ω scaling for Δh exceeds this maximum value, then Δh is capped at the energetically permitted value. Not coincidentally, in the high-$Fr_{Z_\omega}^{-1}$ regime when the maximum displacement is proportional to U_0/N, the Froude number local to the displacement region is of order unity, the scenario under

which highly nonlinear jump-like leewaves occur. In our particular scenario, this regime transition occurs at $Fr_{Z_\omega}^{-1} \approx 3$, and it is for $Fr_{Z_\omega}^{-1} > 3$ that we observe nonlinear jump-like behavior in our simulations. We expect that the U_0/N scaling for Δh will only hold so long as $U_0/N < h_0$, the topographic height, and $U_0/N < H - h_0$, the fluid depth above the topography. If either of these limits is exceeded, then the finite height of the topography or the finite depth of the fluid will influence the motion.

Given this scaling analysis and regime diagram, we predict the principal requirement for internal jump behavior driven by tidal flow is large relative steepness, i.e. large $dh/dx(N/\omega)$. However, given that the jump magnitude, Δh, scales like U/N, large U/N is a second requirement for jumps of significant amplitude. In nondimensional terms, we would not expect the mechanism of internal hydraulic jumps to be important if U/N is smaller than the frictional bottom boundary layer, so we can express this as a type of Reynolds number constraint: $Re_N = U^2/(N\nu_v) >> 1$ for internal jumps to dominate over frictional processes. (In our simulations Re_N varies from 17 in *U2* to 420 in *U10*. In *U2* the jumps are therefore much more strongly affected by friction.) Interestingly, stratification can play a dual role: increasing stratification increases $Fr_{Z_\omega}^{-1}$, making jumps more likely to occur, but reduces U/N, reducing the vertical scale of the isopycnal displacements associated with the jumps.

Finally, we can reexamine our previous qualitative results in terms of the regimes delineated by $Fr_{Z_\omega}^{-1}$. Low $Fr_{Z_\omega}^{-1}$ simulations (e.g. *Gentle slope* or 3ω) did not show any evidence of borelike behavior, in either the snapshots, time-depth profiles, or skewness of the temperature time-derivative. Borelike behavior was seen only for high $Fr_{Z_\omega}^{-1}$.

One question that might be raised is how important is a rapid transition from flat shelf to steep slope? Note that our idealized topography, by including a smooth slope transition on the left and a

discontinuous slope transition on the right, helps to answer this: the discontinuous slope transition on the right does not lead to any internal hydraulic jumps, whereas the smooth transition (to a steeper slope) on the left does. Hence it is the steepness of the slope, not the sharpness of the transition which determines whether an internal hydraulic jump appears. However, the mechanism we have discussed does presume that the flow encounters the steep slope within the tidal cycle, and so the slope transition must be rapid enough that a steep slope, such that $F_{Z_\omega}^{-1}$ is large, is reached within a vertical tidal excursion.

It should be noted that the steepness γ approaches $Fr_{Z_\omega}^{-1}$ in the limit $f < \omega < N$, and so the criterion that $Fr_{Z_\omega}^{-1} > 3$ for borelike behavior could also be expressed as $\gamma > 3$. In practise, for most of the parameters we chose, where ω is not very much greater than f, γ is slightly less than $Fr_{Z_\omega}^{-1}$.

5 Discussion and conclusions

In this paper, motivated by observations from the Kaena Ridge in Hawaii, we have carried out a series of simulations of tidal flow over an isolated ridge, exploring the factors that contribute to overturning behavior on small scales near the shelf-break. We have identified two regimes of behavior near the shelf-break, with the regime transition dependent on $Fr_{Z_\omega}^{-1} = (dh/dx)N/\omega$. For large $Fr_{Z_\omega}^{-1}$, highly nonlinear jump-like lee-waves are found at maximum off-slope flow, with a vertical displacement scale proportional to U/N, such that the jump Froude number is of order unity. When the flow relaxes, the internal jump features propagate toward the slope, leading to well-defined bores propagating up the slope, characterized by negative skewness in the buoyancy time-derivative and associated with overturning and enhanced dissipation. By contrast, for small $Fr_{Z_\omega}^{-1}$, the flow response consists of linear waves, with no jumps or overturning, and the vertical displacement

scale is proportional to the vertical tidal excursion, $(U/\omega)dh/dx$. The FLIP observations from the Hawaiian Ridge fall into the large $Fr_{Z_\omega}^{-1}$ regime of internal jumps and overturning.

Having determined the parameter regime in which the features observed over the Hawaiian Ridge may exist, we now examine whether such features might be expected to have a widespread global distribution. Figure (13a) shows the vertical excursion inverse Froude number, $Fr_{Z_\omega}^{-1} = dh/dxN/\omega$, calculated on a 1/4 degree global scale for the M2 tidal component. N is calculated at the level of the bottom topography from the 1/2 degree gridded WOCE data set of Gouretski and Koltermann (2004). This data set was chosen because particular attention was paid to ensuring stable stratification at depth in the interpolation process. Many of the major ocean ridge systems are associated with sufficiently steep topography that $Fr_{Z_\omega}^{-1} > 3$, and the vertical tidal excursion distance is therefore sufficiently large that internal hydraulic jumps could result. The other prerequisite for such features is large amplitude flow. Figure (13b) shows the amplitude of the M2 barotropic flow component projected onto the direction of the topographic gradient. This calculation was made using the global inverse tide model TPXO6.2 (Egbert and Erofeeva, 2002). Regions of both large-amplitude flow and $Fr_{Z_\omega}^{-1} > 3$ include the Hawaiian ridge, the Mascarene ridge, the Kerguelen plateau, and the entrance to the East China Sea. This examination of the global scale is however limited by its low resolution, but nonetheless provides motivation for examination of tidally driven internal hydraulic jumps in many more locations. One such location is the Oregon Slope, where non-linear effects on the seafloor have recently been reported by Nash et al. (2007). Similar tidally-driven internal hydraulic jumps, have also been observed in fjords (Klymak and Gregg, 2004; Inall et al., 2005), although the dynamics in these regions is modified by the shallow depth of the sill.

In this study we have focused on the qualitative features of the internal hydraulic jump and quantified the parameter space within which this regime occurs. By doing so we have identified

one mechanism by which mixing can be generated local to the topography by the tides. It should be stressed that there are many other mechanisms for generating local tidal mixing, including shear instability in narrow internal tide beams, and wave-wave interactions, especially parametric subharmonic instability. Ultimately we would like to be able to parameterize the mixing generated by tides in an energetically consistent fashion. Simulations such as these cannot provide a complete quantitative answer; a particular caveat is that the ratio of total dissipation to rate of energy conversion in these simulations has been found to be highly sensitive to the viscosity coefficients and resolution of the model. In addition 2D numerical simulations are known to omit important turbulence-generating instabilities. For this reason our focus has been on understanding the mechanism of generating the internal hydraulic jumps, and not on quantifying the mixing due to such features. To fully understand the effect of the internal hydraulic jumps on the energetics of tidal dissipation will therefore require progressively higher resolution 3-dimensional simulations until an asymptotic regime is approached. The simulations in the present study nonetheless provide guidance as to a particular parameter regime where local mixing is important.

Acknowledgments

We would like to thank Rob Pinkel, Steve Garner and Bob Hallberg for their constructive feedback, and two anonymous reviewers whose comments led to a substantial improvement in the manuscript. JK was supported by NSF grant OCE-98-19529 and ONR grant N00014-05-1-0546. SL was supported by Office of Naval Research grant N00014-03-1-0336 and by award NA17RJ2612 from the National Oceanic and Atmospheric Administration, US Department of Commerce. The statements, findings, conclusions and recommendations are those of the authors and do not necessarily reflect the views of the National Oceanic and Atmospheric Administration, or the US Department of Commerce.

References

Aucan, J., Merrifield, M. A., Luther, D. S., Flament, P., 2006. Tidal mixing events on the deep flanks of Kaena Ridge, Hawaii. J. Phys. Oceanogr. 36, 1202–1219.

Balmforth, N., Ierley, G., Young, W., 2002. Tidal conversion by subcritical topography. J. Phys. Oceanogr. 32, 2900–2914.

Bell, T., 1975. Topographically generated internal waves in the open ocean. J. Geophys. Res. 80, 320–327.

Durran, D., 1986. Another look at downslope windstorms. Part I: The development of analogs to supercritical flow in an infinitely deep continously stratified fluid. J. Atmos. Sci. 43, 2527–2543.

Egbert, G., Erofeeva, S., 2002. Efficient inverse modeling of barotropic ocean tides. J. Atmos. Oceanic. Technol. 19, 183–204.

Egbert, G., Ray, R., 2000. Significant dissipation of tidal energy in the deep ocean inferred from satellite altimeter data. Nature 405, 775–778.

Farmer, D. M., Smith, J. D., 1980. Tidal interaction of stratified flow with a sill in Knight Inlet. Deep Sea Res. Part A, 27, 239–245.

Garrett, C., Kunze, E., 2007. Internal Tide Generation in the Deep Ocean. Ann. Rev. of Fluid Mech. 39, 57–87.

Gerkema, T., Staquet, C., Bouruet-Aubertot, P., 2006. Decay of semi-diurnal internal-tide beams due to subharmonic resonance. Geophys. Res. Lett. 33, L08604.

Gouretski, V., Koltermann, K., 2004. WOCE Global Hydrographic Climatology: a technical report. Berichte des Bundesamtes fur Seeschifffahrt und Hydrographie 35.

Inall, M., Rippeth, T., Griffiths, C., Wiles, P., 2005. Evolution and distribution of TKE production and dissipation within stratified flow over topography. Geophys. Res. Lett. 32, Art No. L08607.

Khatiwala, S., 2003. Generation of internal tides in an ocean of finite depth: analytical and numerical calculations. Deep Sea Res. 50, 3–21.

Klymak, J., Gregg, M., 2004. Tidally generated turbulence over the Knight Inlet Sill. J. Phys. Oceanogr. 34, 1135–1151.

Klymak, J., Moum, J., Nash, J., Kunze, E., Girton, J., Carter, G., Lee, C., Sanford, T., Gregg, M., 2006. An estimate of tidal energy lost to turbulence at the Hawaiian ridge. J. Phys. Oceanogr. 36, 1148–1164.

Klymak, J. M., Pinkel, R., Rainville, L. N., 2007. Direct breaking of the internal tide near topography: Kaena Ridge, Hawaii, in review, *J. Phys. Oceanogr.*

Legg, S., 2004. Internal tides generated on a corrugated continental slope. Part II: Along-slope barotropic forcing. J. Phys. Oceanogr. 34, 1824–1834.

Legg, S., Adcroft, A., 2003. Internal wave breaking at concave and convex continental slopes. J. Phys. Oceanogr. 33, 2224–2246.

Legg, S., Huijts, K., 2006. Preliminary simulations of internal waves and mixing generated by finite amplitude tidal flow over isolated topography. Deep Sea Research, Part II 53, 140–156.

Levine, M. D., Boyd, T. J., 2006. Tidally-forced internal waves and overturns observed on a slope: results from the HOME survey component. J. Phys. Oceanogr. 36, 1184–1201.

Llewellyn Smith, S., Young, W., 2003. Tidal conversion at a very steep ridge. J. Fluid. Mech. 495, 175–191.

Long, R., 1953. Some aspects of the flow of stratified fluids. I. A theoretical investivation. Tellus 5, 42–57.

Long, R., 1954. Some aspects of the flow of stratified fluids. II. Experiments with a two-fluid system. Tellus 6, 97–115.

Marshall, J., Adcroft, A., Hill, C., Perelman, L., Heisey, C., 1997. A finite-volume, incompressible Navier-Stokes model for studies of the ocean on parallel computers. J. Geophys. Res. 102 (C3), 5753–5766.

Nash, J., Alford, M., Kunze, E., Martini, K., Kelley, S., 2007. Hotspots of deep ocean mixing on the oregon continental slope. Geophys. Res. Lett. 34, L01605, doi:10.1029/2006GL028170.

Polzin, K., Toole, J., Ledwell, J., Schmitt, R., 1997. Spatial variability of turbulent mixing in the abyssal ocean. Science 276, 93–96.

Rudnick, D., Boyd, T., Brainard, R., Carter, G., Egbert, G., Gregg, M., Holloway, P., Klymak, J., Kunze, E., Lee, C., Levine, M., Luther, D., Martin, J., Merrifield, M., Moum, J., Nash, J., Pinkel, R., Rainville, L., Sanford, T., 2003. From tides to mixing along the Hawaiian ridge. Science 301, 355–357.

St Laurent, L., Stringer, S., Garrett, C., Perrault-Joncas, D., 2003. The generation of internal tides at abrupt topography. Deep Sea Res. 50, 987–1003.

Wunsch, C., Ferrari, R., 2004. Vertical mixing, energy and the general circulation of the oceans. Ann. Rev. of Fluid Mech. 36, 281–314.

List of Figures

Simulation	U_0	N^2	dh/dx_{max}	$\gamma_{max} = dh/dx_{max}/s$	$Fr_{Z_\omega} = \omega/(Ndh/dx_{max})$	U_0/N
Realistic	$5cm/s$	variable	0.2	4	0.3	21m
Steep slope	$5cm/s$	$5.69 \times 10^{-6}s^{-2}$	0.2	4	0.3	21m
Medium slope	$5cm/s$	$5.69 \times 10^{-6}s^{-2}$	0.1	2	0.59	21m
Gentle slope	$5cm/s$	$5.69 \times 10^{-6}s^{-2}$	0.06	1.2	0.99	21m
SteepU10	$10cm/s$	$5.69 \times 10^{-6}s^{-2}$	0.2	4	0.3	42m
SteepU2	$2cm/s$	$5.69 \times 10^{-6}s^{-2}$	0.2	4	0.3	8m
$2N^2$	$5cm/s$	$1.14 \times 10^{-5}s^{-2}$	0.2	5.8	0.21	15m
$4N^2$	$5cm/s$	$2.28 \times 10^{-5}s^{-2}$	0.2	8.2	0.15	10m
$8N^2$	$5cm/s$	$4.56 \times 10^{-5}s^{-2}$	0.2	11.7	0.10	5m
$N^2/4$	$5cm/s$	$1.42 \times 10^{-6}s^{-2}$	0.2	2.0	0.6	42m
2ω	$5cm/s$	$5.69 \times 10^{-6}s^{-2}$	0.2	1.8	0.6	21m
3ω	$5cm/s$	$5.69 \times 10^{-6}s^{-2}$	0.2	1.1	0.9	21m
$\omega/2$	$5cm/s$	$5.69 \times 10^{-6}s^{-2}$	0.2	7.0	0.15	21m

Table 1: Values of topographic and flow parameters for the numerical simulations.

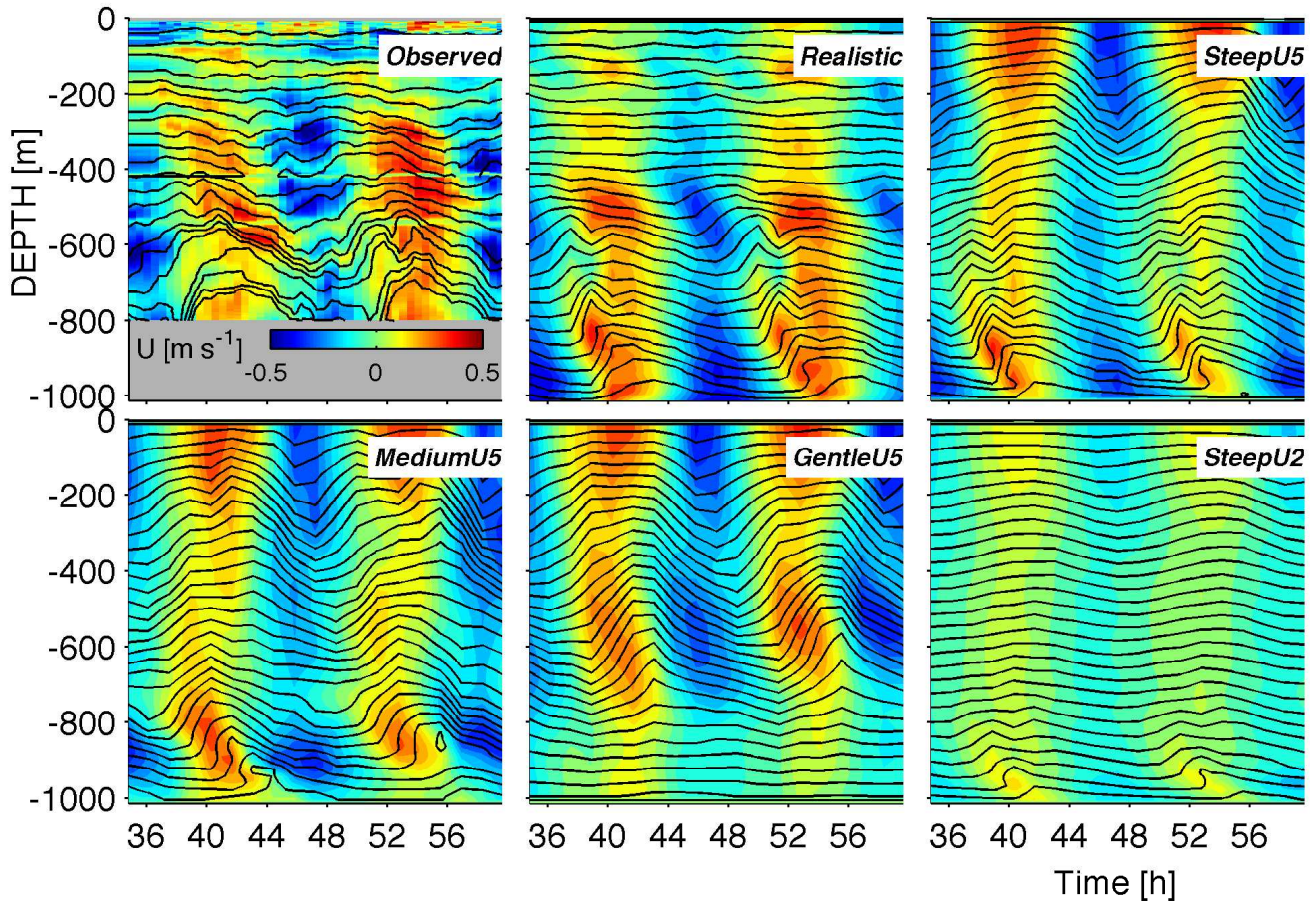

Figure 1: Time-depth sections showing the cross-slope component of velocity, with density contours overlain, at a location near the top of the shelf-break. The top left panel shows values observed from FLIP, while other panels show model-simulated values, with details of the different simulations given in the Table and in section 2.

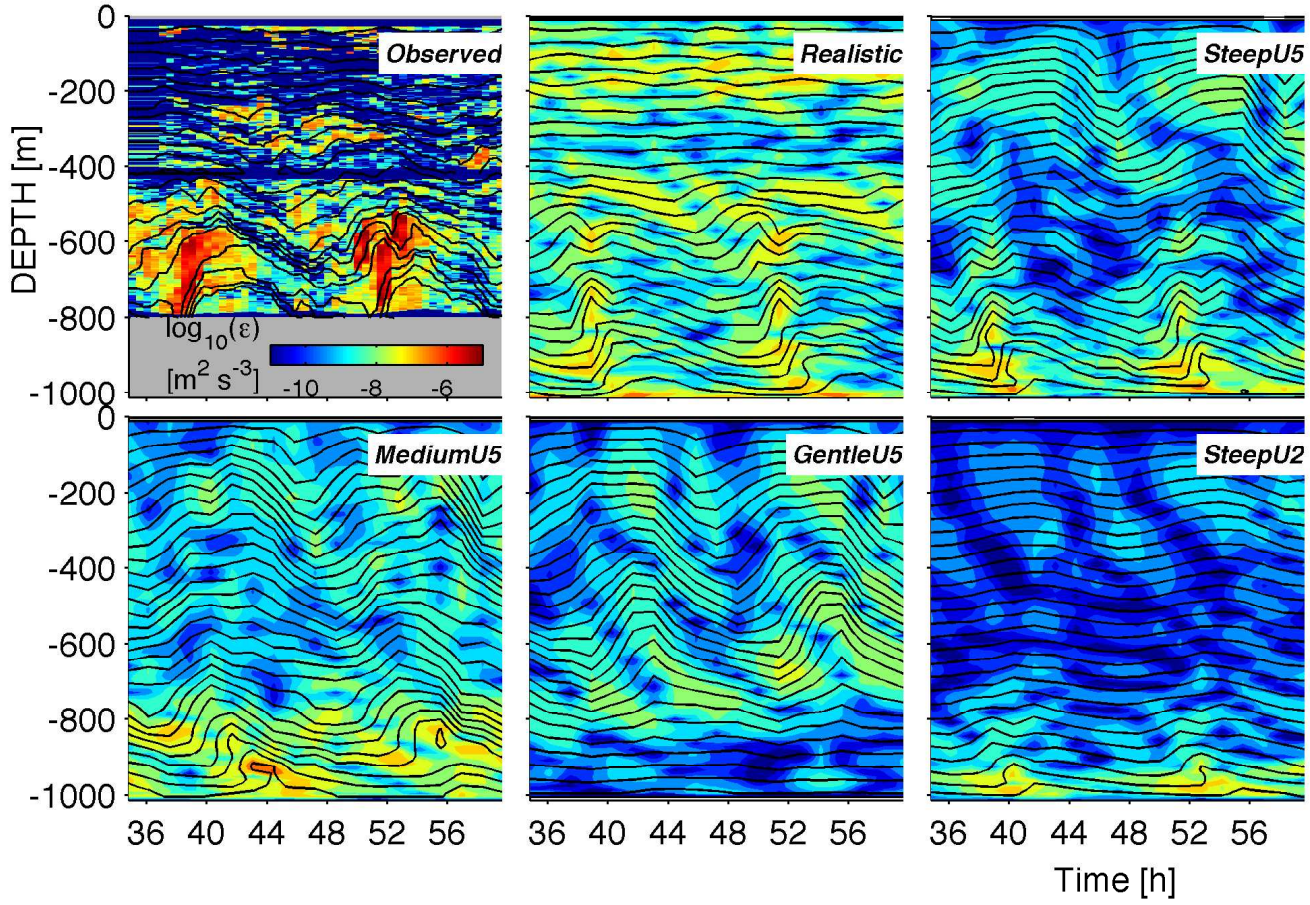

Figure 2: Time-depth sections showing the kinetic energy dissipation, with density contours overlain, at a location near the top of the shelf-break. The top left panel shows values observed from FLIP, while other panels show model-simulated values, with details of the different simulations given in the Table and in section 2.

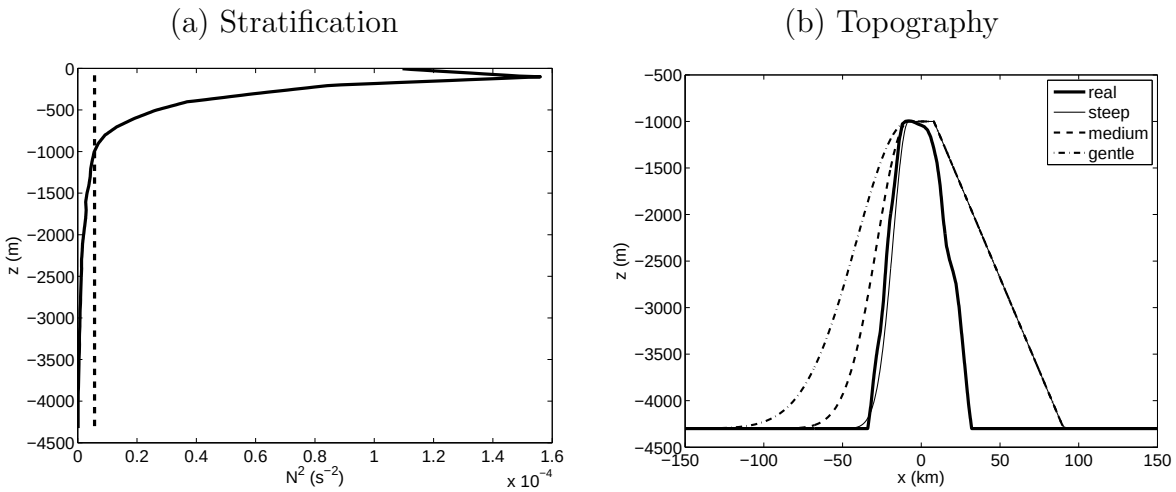

Figure 3: (a) The stratification N^2 and (b) the topography used in the different simulations. In (a) the solid line shows the real N^2 profile, while the dashed line shows the constant N^2 profile used in most of the idealized calculations, which matches the real N^2 value at the top of the topography. Four other idealized calculations have $N^2 = 2\times, 4\times$, $8\times$ and $1/4$ of this value. In (b) the thick solid line shows the real topography, and the other lines show different idealized topographies described in the text. Note that all idealized calculations have the same topography for $x > 0$, with much gentler slope than the real topography.

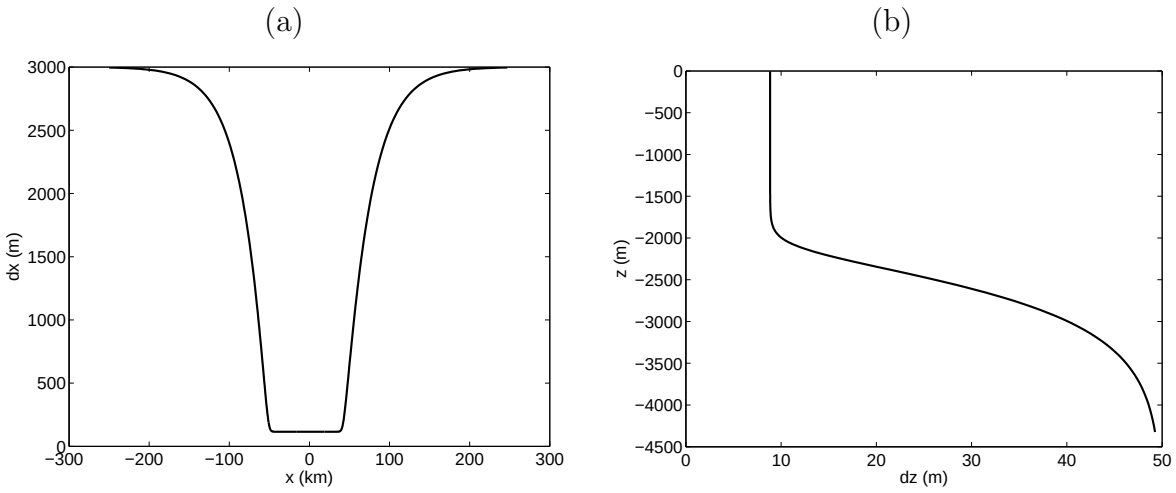

Figure 4: The resolution used in all the simulations: (a) Δx, (b) Δz. High resolution is concentrated within the region $-50km < x < 50km$, $-2000m < z < 0$

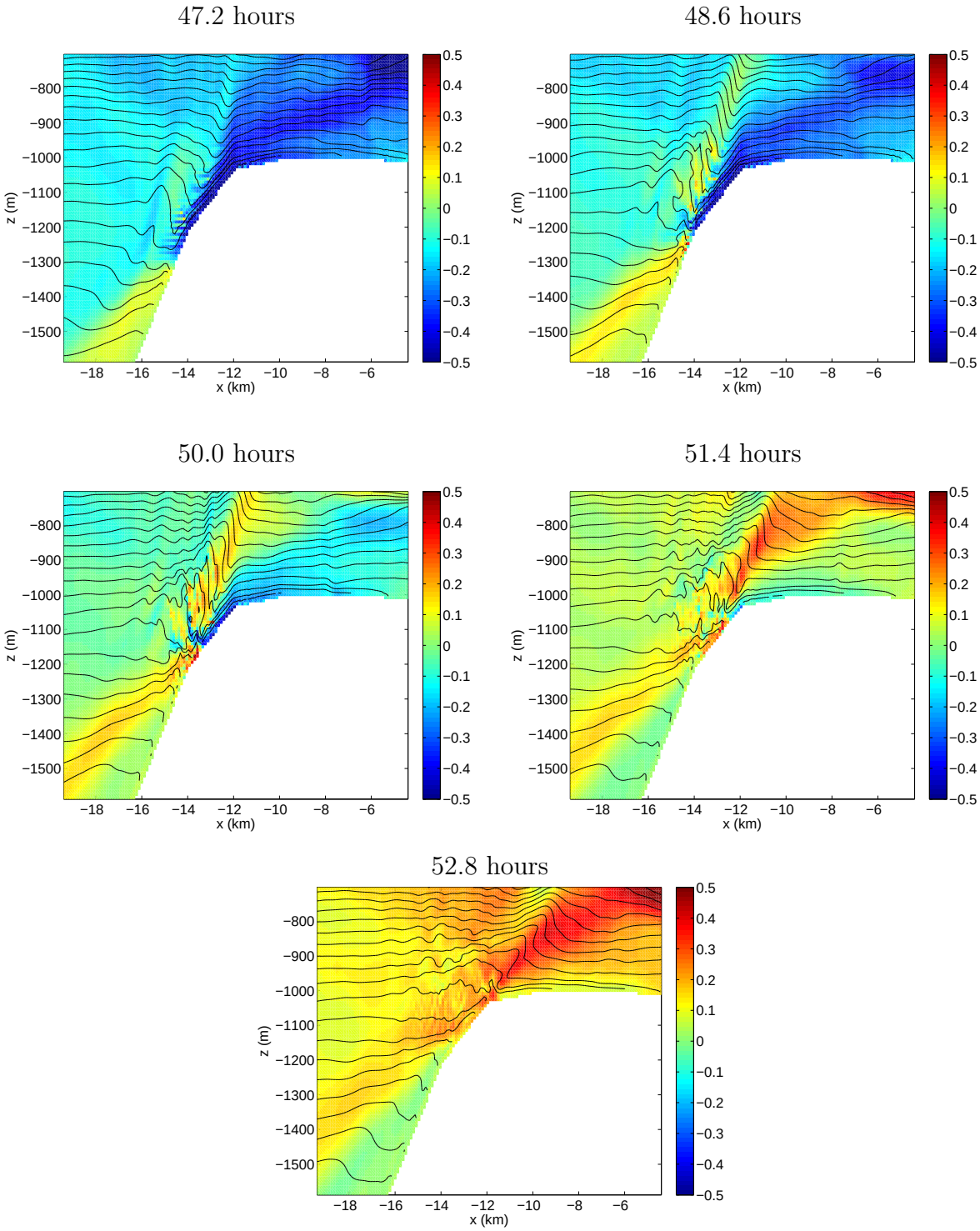

Figure 5: Snapshots of the cross-shelf velocity (color, m/s) and density for the *Realistic* simulation, near the shelfbreak, over the course of approximately half a tidal cycle. Maximum off-slope tide is at 46.4 hours, while maximum onslope tide is at 52.6 hours.

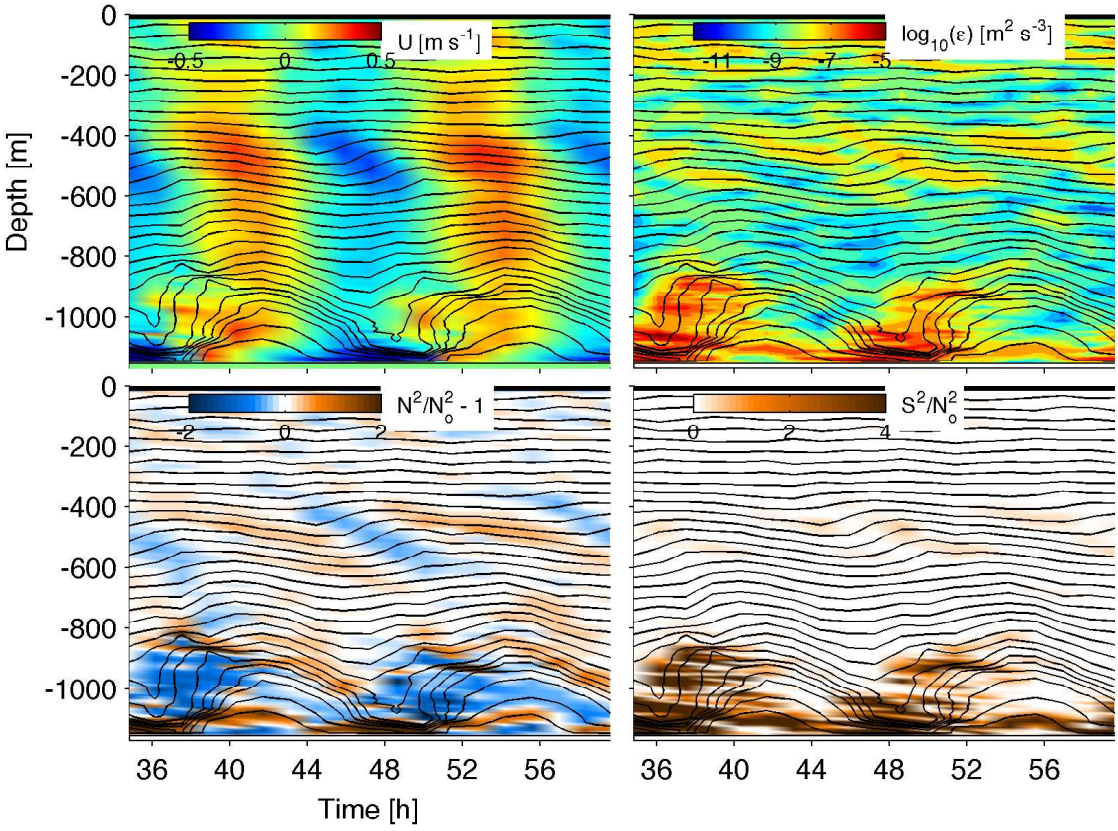

Figure 6: Time-depth plots from the *Realistic* simulation at a location of depth $h = -1150m$, to the left of the ridge, with density contours overlain.

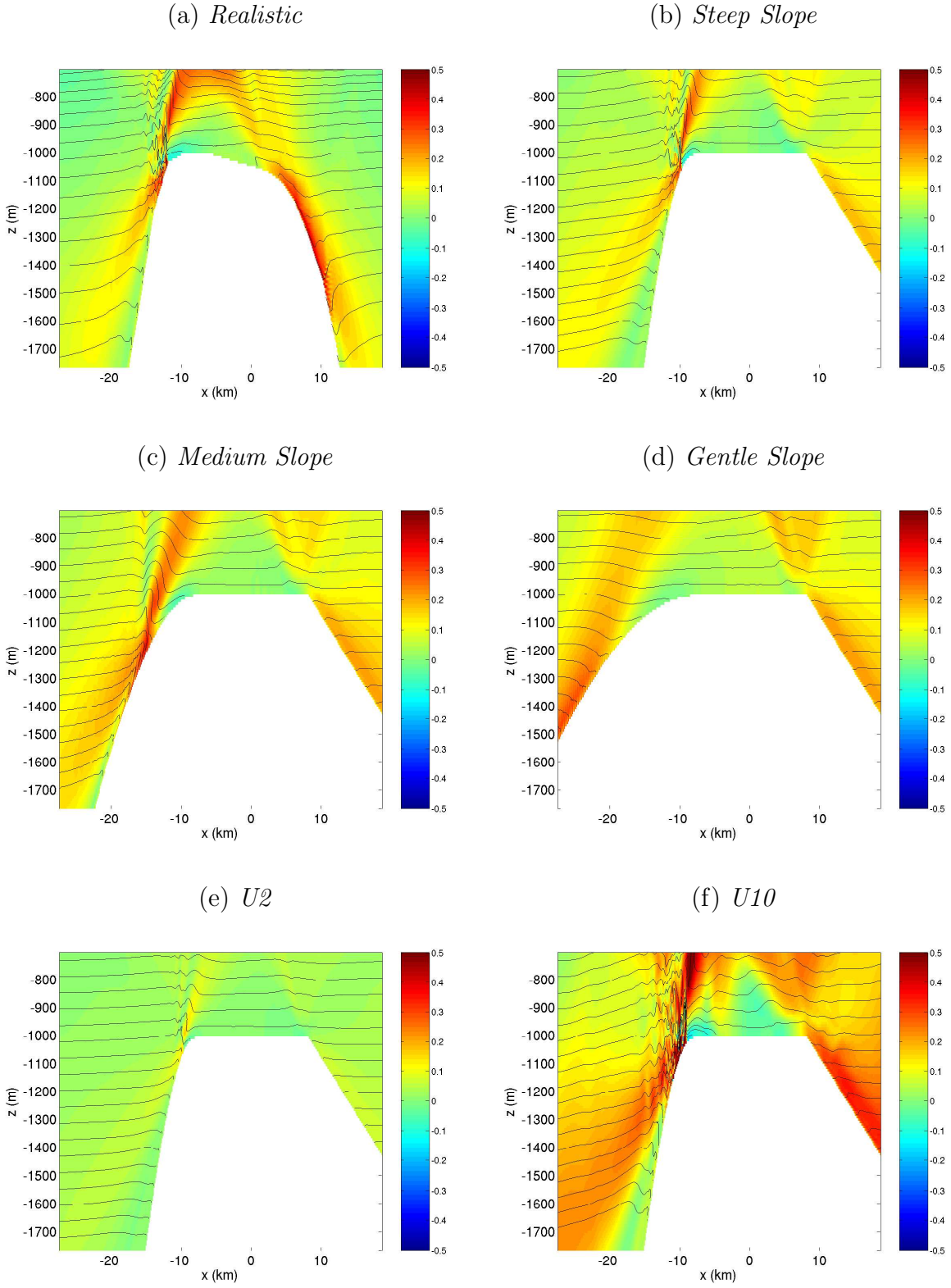

Figure 7: Snapshots of the cross-slope velocity field (color) and buoyancy (black contours) at a time 1.12 tidal periods after the beginning of the simulation for (a) *Realistic* topography and stratification, $U_0 = 5cm/s$, (b) *Steep slope*, $U_0 = 5cm/s$, (c) *Medium slope*, $U_0 = 5cm/s$, (d) *Gentle*

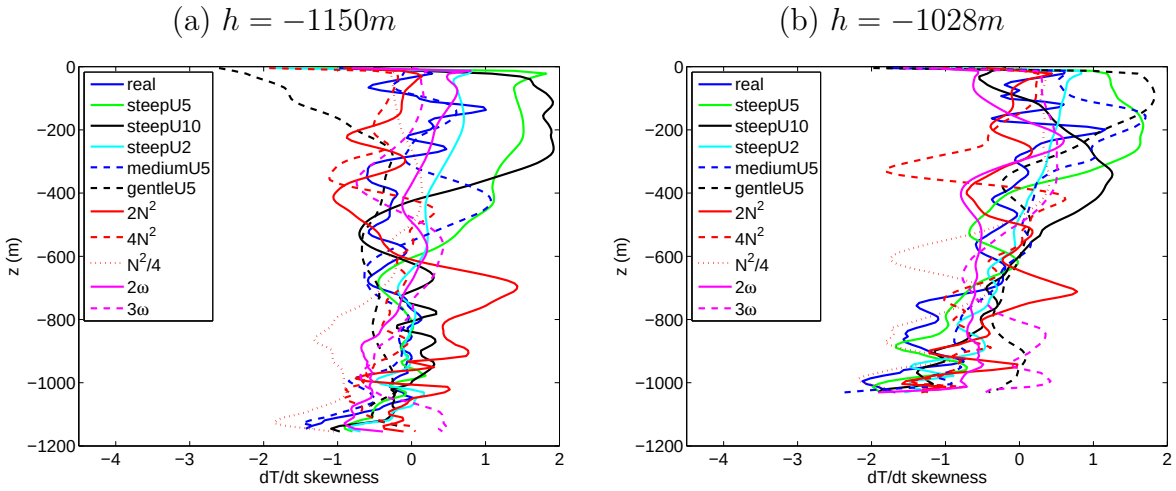

Figure 8: The skewness of the temperature time-derivative, shown as a function of depth for two locations where the topographic depth is (a) -1150m and (b) -1028m, shown for all idealized topography runs. Dashed lines indicate simulations with $Fr_{Z_\omega} > 0.3$ (see section 4)

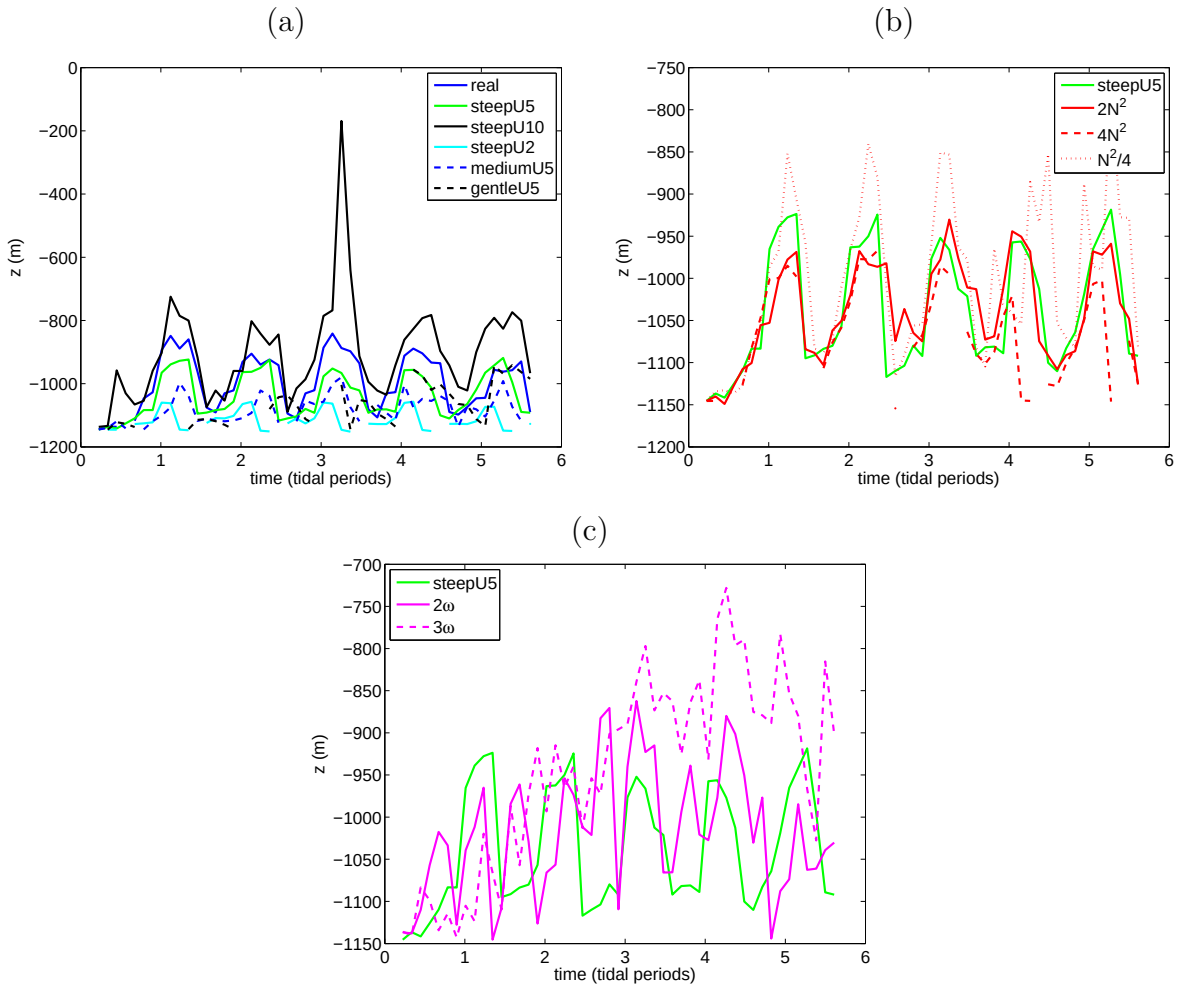

Figure 9: Comparison of the height at which gradient Richardson number is equal to 1, for all runs, at a location where the topographic depth is -1150m. (a) Dependence on variations in topography and U_0, (b) dependence on variations in N^2 and (c) dependence on variations in ω.

(a) *Realistic*

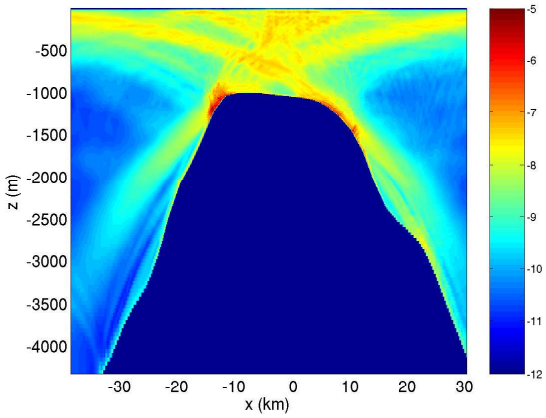

(b) *Steep Slope*

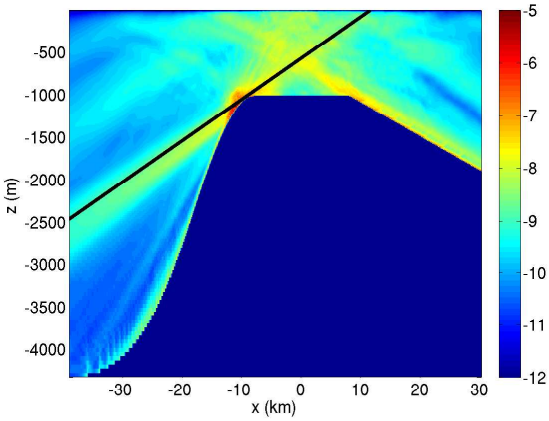

(c) *Medium Slope*

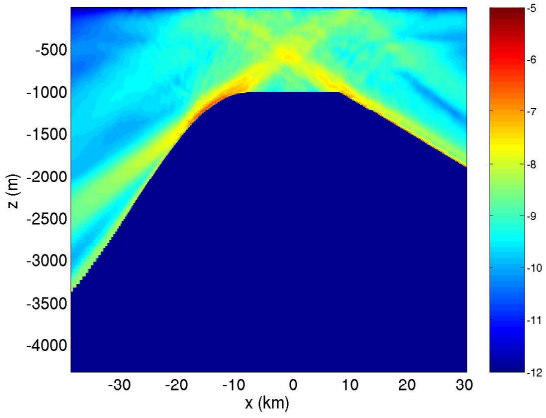

(d) *Gentle Slope*

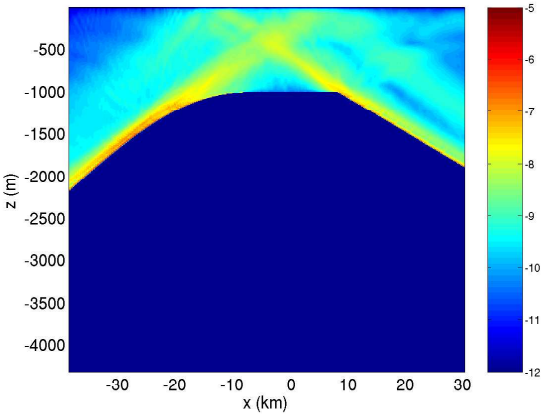

(e) *U2*

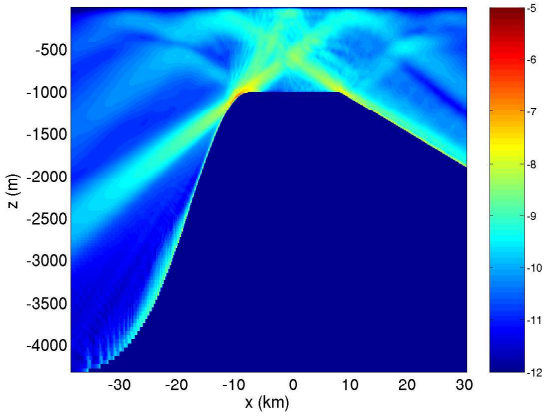

(f) *U10*

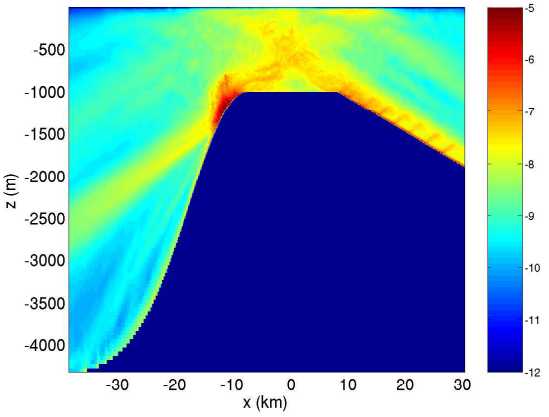

Figure 10: Time-averaged dissipation ϵ: (a) *Realistic* topography and stratification, $U_0 = 5cm/s$; (b) *Steep slope*, $U_0 = 5cm/s$; (c) *Medium slope*, $U_0 = 5cm/s$; (d) *Gentle slope*, $U = 5cm/s$; (e) *SteepU2*, $U_0 = 2cm/s$; (f) *SteepU10*, $U = 10cm/s$. The M2 internal tide characteristic emanating

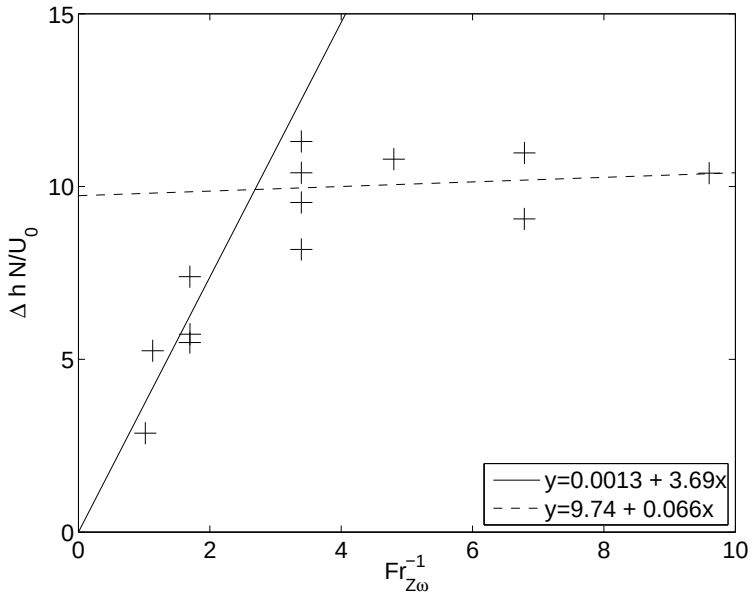

Figure 11: The maximum downward displacement of isopycnals originating over the shelf (Δh), nondimensionalized by U_0/N, shown plotted against $Fr_{Z_\omega}^{-1}$. The two lines show least squares best fits calculated separately for the points with $Fr_{Z_\omega}^{-1} < 3$ (solid) and $Fr_{Z_\omega}^{-1} > 3$ (dashed). For $Fr_{Z_\omega}^{-1} < 3$, there is a linear relationship: $\Delta hN/U_0 \approx 3.7 Fr_{Z_\omega}^{-1}$, while for $Fr_{Z_\omega}^{-1} > 3$, $\Delta hN/U_0$ is independent of $Fr_{Z_\omega}^{-1}$, and approximately constant, with a value of $\Delta hN/U_0 \approx 10$.

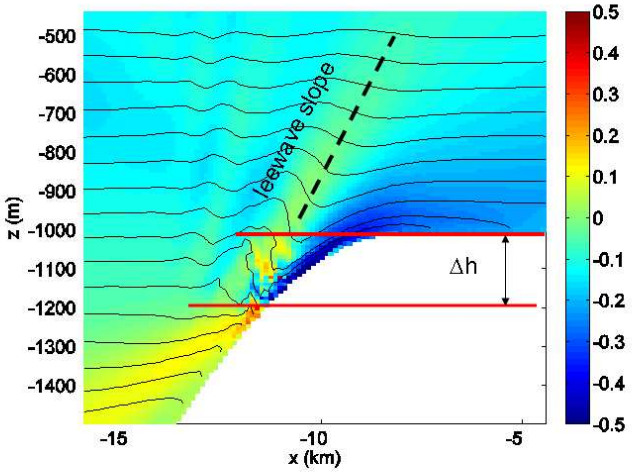

Figure 12: A schematic, based on the *Steep* slope simulation, showing the maximum downward vertical displacement of the isopyncals Δh and the slope of the leewave, defined by the horizontal velocity maximum. Horizontal velocity is shown in color, buoyancy in black contours.

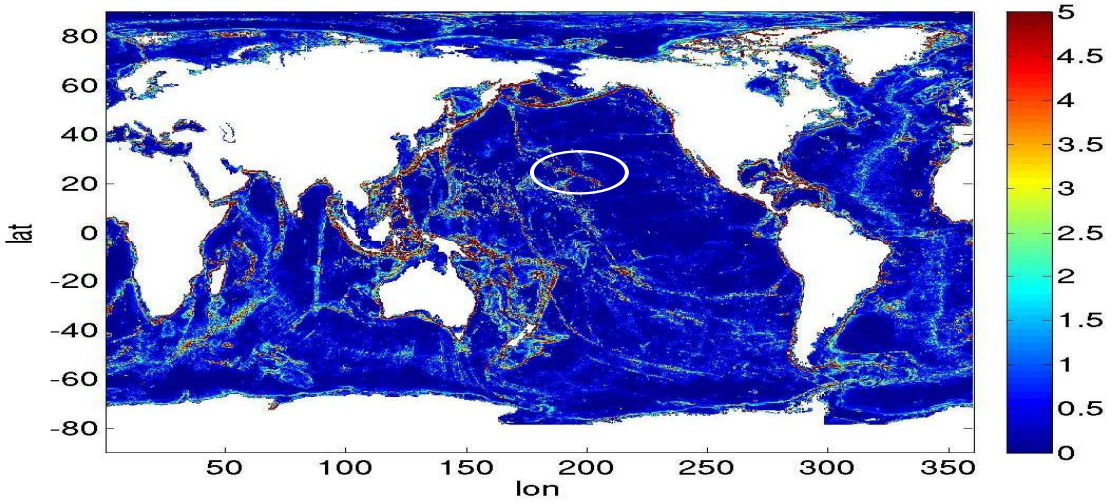

(a)

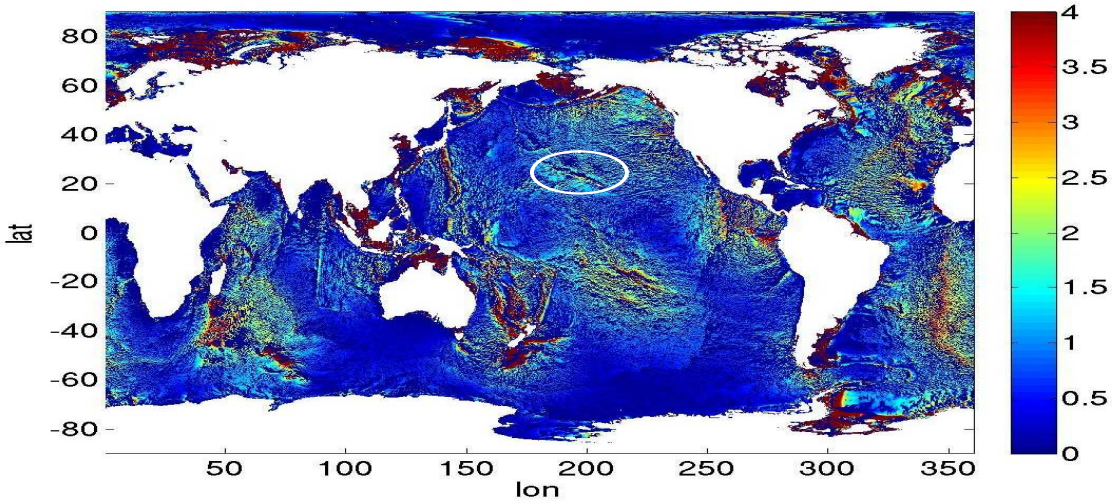

(b)

Figure 13: (a) The M2 tidal excursion inverse Froude number $Fr_{Z\omega}^{-1} = dh/dxN/\omega$ on 1/2 degree spatial scale, where N is the stratification just above the topography, obtained using Koltermann and Gouretsky 1/2 degree gridded WOCE hydrography. (The colorscale has been truncated to highlight regions where $Fr^{-1} > 3$). (b) The M2 tidal velocity amplitude (in cm/s), projected onto the topographic gradient. (The color scale has been truncated to highlight mid-ocean values). In both figures the Hawaiian ridge is marked by a white oval.